Environ Fluid Mech (2011) 11:499–516
DOI 10.1007/s10652-010-9192-x

ORIGINAL ARTICLE

Near-critical free-surface flows: real fluid flow analysis

Oscar Castro-Orgaz · Hubert Chanson

Received: 8 May 2010 / Accepted: 13 August 2010 / Published online: 11 September 2010

Abstract An open channel flow with a flow depth close to the critical depth is characterised by a curvilinear streamline flow field that results in steady free surface undulations. Near critical flows of practical relevance encompass the undular hydraulic jump when the flow changes from supercritical ($F > 1$) to subcritical ($F < 1$), and the undular weir flow over broad-crested weirs where the flow changes from subcritical ($F < 1$) to supercritical ($F > 1$). So far these flows were mainly studied based on ideal fluid flow computations, for which the flow is assumed irrotational and, thus, shear forces are absent. While the approach is accurate for critical flow conditions ($F = 1$) in weir and flumes, near-critical flows involve long distances reaches, and the effect of friction on the flow properties cannot be neglected. In the present study the characteristics of near-critical free-surface flows are reanalysed based on a model accounting for both the streamline curvature and friction effects. Based on the improved model, some better agreement with experimental results is found, thereby highlighting the main frictional features of the flow profiles.

Keywords Open channels · Near-critical flows · Frictional effects · Hydraulic jump · Transitional flow · Turbulence · Undular flow

List of symbols

b Channel width
C_f Skin friction coefficient (–)

O. Castro-Orgaz (✉)
Instituto de Agricultura Sostenible, Consejo Superior de Investigaciones Cientificas,
Finca Alameda del Obispo, 14080 Cordoba, Spain
e-mail: oscarcastro@ias.csic.es

H. Chanson
Hydraulic Engineering, School of Civil Engineering, The University of Queensland,
Brisbane, QLD 4072, Australia
e-mail: h.chanson@uq.edu.au

F	Froude number (–)
f	Friction factor (–)
g	Acceleration of gravity (m/s^2)
H	Specific energy (m)
H_o	Free surface streamline specific energy (m)
h	Flow depth measured normal to channel bottom (m)
i	Streamline inclination (rad)
$\overline{p}$	Time-averaged pressure (N/m^2)
q	Unit discharge (m^2/s)
L	Crest length (m)
R_h	Hydraulic radius (m)
R	Reynolds number (–)
S_f	Friction slope (–)
S_o	Bed slope (–)
S	Specific momentum (m^2)
$\overline{u}$	Time-averaged turbulent velocity parallel to bottom (m/s)
U	Cross-sectional averaged flow velocity (m/s)
U_M	Maximum flow velocity at the outer edge of boundary layer (m/s)
V	Magnitude of potential flow velocity (m/s)
$\overline{v}$	Time-averaged turbulent velocity normal to bottom (m/s)
x	Streamwise distance (m)
y	Distance measured normal to channel bed (m)
z''	Bed curvature (m^{-2})
α	Angle of bottom with horizontal (rad)
ρ	Fluid density (N/m^3)
γ	Specific weight (N/m^3)
η	Dimensionless distance normal to channel bottom (–)
τ	Reynolds stress (N/m^2)
τ_o	Boundary shear stress (N/m^2)
ν	Kinematic viscosity (m/s^2)
κ	von Karman constant (–)
$\delta*$	Boundary layer displacement thickness (m)
θ	Boundary layer momentum thickness (m)
ϕ	Depth-averaged non-hydrostatic energy coefficient (–)
ψ	Depth-averaged non-hydrostatic momentum coefficient (–)

Subscripts

1	Approach flow
c	Critical flow

1 Introduction

Water flow in natural streams with small slopes near the critical slope results in an undulating flow pattern, whose wave amplitude is typically larger that the standard computation resulting from the gradually-varied flow theory. An open channel with a flat bottom operating near critical flow conditions is characterized by the appearance of steady free surface undulations, although these may appear as well in irregular natural streams with dune-type bed

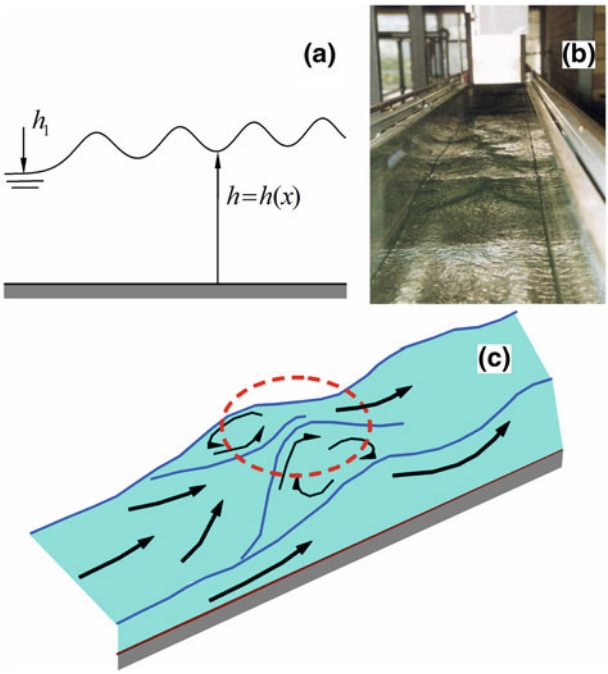

Fig. 1 A near-critical free surface flow: the undular hydraulic jump **a** typical centerline profile, **b** undular hydraulic jump looking downstream (undular jump type C) $F_1 = 1.36$, **c** 3D flow pattern for $F_1 > 1.2$ to 1.25 (after [13])

forms. The analysis and computation of near-critical flow is then a problem of interest for environmental fluid mechanics applications. Two of the most relevant types of near critical flows are the undular hydraulic jump and the undular weir flow [9]. The undular hydraulic jump is a transition from supercritical ($F > 1$) to subcritical ($F < 1$) flow in the form of steady waves, typically if F_1 is close to unity (Fig. 1), with $F_1 =$ approach Froude number [9]. For $F_1 < 1.2$ to 1.25, the free surface profile is typically two-dimensional, whereas for $F_1 > 1.2$ to 1.25 shockwaves appears and the flow turns into highly three-dimensional features [13,8]. Figure 1 illustrates an undular hydraulic jump with some lateral shock waves. Fawer [15] first analyzed this problem from a fundamental approach, although it was earlier observed by Darcy and Bazin [14]. Fawer treated undular hydraulic jumps with a Boussinesq-type energy equation [15,4,6]. He did not consider the transition from $F > 1$ to $F < 1$ upstream the first wave crest, but experimentally detailed the undular flow features. A number of works analyzed the undular jump using the potential flow theory [15,2,19,21] whereas Montes [25] and Montes and Chanson [27] explicitly discussed the importance of wall friction, and, thus, of the real fluid flow effects.

The undular weir flow is a transition from a subcritical ($F < 1$) to supercritical ($F > 1$) flow in the form of steady waves, typically if $H_o/L < 0.15$ [9,26,12], with $H_o =$ upstream head above on the weir crest and $L =$ crest length. The flow over the broad-crested weir for $H_o/L < 0.5$ is usually modeled by a parallel-streamline flow approach [26], whereas the free surface undulations appearing on the weir crest for $H_o/L < 0.15$ invalidate this type of approach. The streamlined broad-crested weir has the additional complication that the boundary layer is partially developed along the crest. Further, boundary layer methods for

broad-crested weir flow rely on zero pressure gradients approximations [17], incompatible with the steadily changing non- hydrostatic pressure gradient from adverse to favorable, and viceversa, induced by the free surface undulations [25].

Chanson [9] presented a detailed analysis of both flow types based on ideal fluid flow calculations and physical data, but the real fluid flow effects are relevant. In the literature, few attempts are available to the analysis of near-critical free surface flows including wall-friction features, among which Montes [25] and Montes and Chanson [27]. Note that there are other types of undular flows including the undular surges and tidal bores [20], but the effects of boundary friction is believed to be more pronouced in undular hydraulic jumps and undular flows above a broad-crested weir. In this paper, the hydraulic analysis of both undular hydraulic jumps and undular weir flows presented by Chanson [9] is extended following Montes [25].The free surface characteristics of both undular jumps and undular weir flows are considered based on the inclusion of boundary friction in the governing equations. The real fluid flow results are compared with the ideal fluid flow theory. The real fluid flow effects in undular jumps with upstream, fully-developed boundary layer flow are investigated. The results are compared with the integration of the Reynolds equations based on a k–ε model. The developing boundary layer flow over broad-crested weirs is analyzed including the friction term, and the results for the boundary layer development with adverse-favorable pressure gradients are compared with the numerical results using zero-pressure gradient boundary layer equations.

2 Governing equations

The time-averaged velocity $\bar{u}$ parallel to the channel bottom in 2D incompressible free surface flow may be approximated to the lowest order by its depth-averaged value U

$$\bar{u} = U = \frac{q}{h} \tag{1}$$

with q = unit discharge and h = flow depth. Using the time-averaged form of the 2D continuity equation

$$\frac{\partial \bar{u}}{\partial x} + \frac{\partial \bar{v}}{\partial y} = 0 \tag{2}$$

the time-averaged velocity $\bar{v}$ normal to the channel bottom is, after integration

$$\bar{v} = -\int_0^y \frac{\partial U}{\partial x} \mathrm{d}y = U h' \eta \tag{3}$$

with $h' = \mathrm{d}h/\mathrm{d}x$ and $\eta = y/h$, where x = streamwise coordinate along the channel bottom and y = coordinate normal to x, positive upwards. The momentum balance perpendicular to the channel bottom is

$$\bar{u}\frac{\partial \bar{v}}{\partial x} + \bar{v}\frac{\partial \bar{v}}{\partial y} = -\frac{1}{\rho}\frac{\partial \bar{p}}{\partial y} + \frac{1}{\rho}\frac{\partial \tau}{\partial x} - g\cos\alpha \tag{4}$$

where $\bar{p}$ = time-averaged pressure, τ = tangential Reynolds stress and α = bottom slope angle. The convective acceleration term in Eq. 4 may be expressed with the aid of Eq. 2 as

$$\bar{u}\frac{\partial \bar{v}}{\partial x} + \bar{v}\frac{\partial \bar{v}}{\partial y} = \bar{u}^2 \frac{\partial}{\partial x}\left(\frac{\bar{v}}{\bar{u}}\right) \tag{5}$$

Inserting Eqs. 1, 3 and 5 into Eq. 4, and noting that $\partial\tau/\partial x << \partial\bar{p}/\partial y$ and $\partial\tau/\partial y$[5], results after integration

$$\frac{\bar{p}}{\gamma} = (h-y)\cos\alpha + \frac{U^2}{2g}\left(hh'' - h'^2\right)\left[1-\eta^2\right] \tag{6}$$

with $h'' = \mathrm{d}^2h/\mathrm{d}x^2$. Equation 6 is the pressure distribution in wavy 2D free surface flows [25,26,29]. It is worth pointing out that Eq. 6 was obtained on the assumptions that (i) the x-direction velocity distribution may be approximated by its depth-averaged value $\bar{u} = q/h$, a reasonable approximation for Reynolds numbers R$\rightarrow\infty$. Bose and Dey [5] and Montes and Chanson [27] considered power law profiles for the velocity distribution. Although more simple that the law of the wall, the power law velocity distribution gives results very close to the log-law [16,12]; and (ii) the turbulence shear stress are dominant in the y-direction $\partial\tau/\partial x \ll \partial\tau/\partial y$. Thus, Eq. 6 is not limited to irrotational flows as implicit in other Boussinesq-type developments based on a potential flow approach [2,22–24].

The momentum balance in the x-direction is

$$\bar{u}\frac{\partial\bar{u}}{\partial x} + \bar{v}\frac{\partial\bar{u}}{\partial y} = -\frac{1}{\rho}\frac{\partial\bar{p}}{\partial x} + \frac{1}{\rho}\frac{\partial\tau}{\partial y} + g\sin\alpha \tag{7}$$

Inserting Eqs. 1, 3 and

$$\bar{u}\frac{\partial\bar{u}}{\partial x} + \bar{v}\frac{\partial\bar{u}}{\partial y} = \frac{\partial\bar{u}^2}{\partial x} + \frac{\partial\bar{u}\bar{v}}{\partial y} \tag{8}$$

into the streamwise momentum balance Eq. 7 and integrating from $y = 0$ to $y = h$ yields

$$\frac{\mathrm{d}S}{\mathrm{d}x} = h\left(S_o - S_f\right) \tag{9}$$

where S_f = friction slope, S_o = bed slope and S = specific momentum given by

$$S = \int_0^h \left[\frac{\bar{u}^2}{g} + \frac{\bar{p}}{\gamma}\right]\mathrm{d}y = \frac{h^2}{2} + \frac{q^2}{gh}\left(1 + \frac{hh'' - h'^2}{3}\right) \tag{10}$$

Expanding the term $\mathrm{d}S/\mathrm{d}x$ in Eq. 9, and integrating the result after elimination of the term h in the RHS of Eq. 9 yields

$$\frac{\mathrm{d}H}{\mathrm{d}x} = S_o - S_f \tag{11}$$

where H = depth-averaged specific energy, given by

$$H = \frac{1}{h}\int_0^h \left[\frac{\bar{u}^2+\bar{v}^2}{2g} + \frac{\bar{p}}{\gamma} + y\cos\alpha\right]\mathrm{d}y = h + \frac{q^2}{2gh^2}\left(1 + \frac{2hh'' - h'^2}{3}\right) \tag{12}$$

Thus, the depth-averaged mean energy balance is equivalent to the x-momentum balance. The system of Eqs. 9 and 10 is fully equivalent to Eqs. 11 and 12, and the same results may be obtained using either energy or momentum considerations as originally noted Serre [29]. The extended specific energy and momentum may be expressed as

$$H = h + \phi\frac{q^2}{2gh^2} \tag{13}$$

$$S = \frac{h^2}{2} + \psi\frac{q^2}{gh} \tag{14}$$

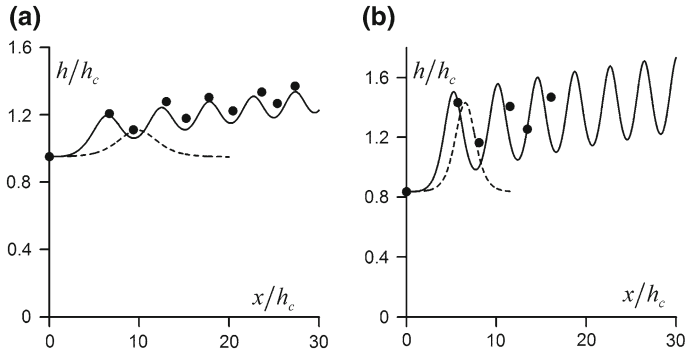

Fig. 2 Transition from F > 1 to F < 1: undular hydraulic jump profile $h/h_c(x/h_c)$ for **a** $F_1 = 1.08$ from (—) Real fluid flow theory, (- - -) Ideal fluid flow and (•) experimental data ([7], Test HCUJ10b, $q = 0.08\,m^2/s$, $h_1 = 0.0824$ m, $\alpha = 0.229°$), **b** $F_1 = 1.31$ from (—) Real fluid flow theory, (- - -) Ideal fluid flow and (•) experimental data ([7], Test HCUJ5c, $q = 0.12\,m^2/s$, $h_1 = 0.095$ m, $\alpha = 0.382°$)

differing from the classical expressions for parallel-streamline flow $H = h + q^2/(2gh^2)$ and $S = (h^2/2)+q^2/(gh)$ in the coefficients ϕ and ψ. These coefficients may reach values greater or lower than unity, depending on the free surface slope and curvature. Based on the solution of Eqs. 11 and 12 its magnitude will be investigated herein for near-critical flows.

3 Undular Hydraulic Jump

The undular hydraulic jump is a transitional flow from supercritical F > 1 to subcritical F < 1 open channel flows in the form of an undulating free-surface profile. For comparative purposes between the theoretical model described above and experimental data, the detailed set of experiments by Chanson [7] is considered. Experimental data for an undular jump of $F_1 = 1.08$ (Test HCUJ10b) and $F_1 = 1.31$ (Test HCUJ5c) are presented in Fig. 2a and b respectively. The system of differential Eqs. 11 and 12 was solved for the unknowns $h(x)$ and $H(x)$ with a 4th-order Runge-Kutta method. The boundary conditions are taken at the toe of the undular jump (subscript 1, Fig. 1) as $h_1 = h(x = 0) = F_1^{-2/3}$, $h_1' = h'(x = 0) = 0$ and $h_1'' = h''(x = 0) = 0$. The value of $H_1 = H(x = 0)$ is deduced from Eq. 12 with $h' = h'' = 0$. This set of boundary conditions states hydrostatic pressure distribution at the coordinate origin $x = 0$.

The friction slope in Eq. 11 is given based on the Darcy-Weisbach equation by [26,10]

$$S_f = \frac{f}{4h}\frac{U^2}{2g} \tag{15}$$

where f = Darcy-Weisbach friction factor. The differential system defining the free surface profile $h = h(x)$ have no analytical solution as in some irrotational flow cases [2]. Thus, Eqs. 11 and 12 need to be solved numerically for turbulent, near-critical, free surface flow. Herein, f is considered for turbulent smooth flow using the proposal of Haaland [31]

$$f = \left[-1.8\log_{10}\left(\frac{6.9}{4R_1}\right)\right]^{-2} \tag{16}$$

where $R_1 = q/\nu$ = approach flow Reynolds number and ν = kinematic viscosity. The accuracy of Eq. 16 as compared to the Colebrook-White equation is ±2%: i.e., adequate

for practical purposes. The numerical results for $F_1 = 1.08$ are inserted in Fig. 2a showing that the Boussinesq system Eqs. 11 and 12, with Haaland's equation for turbulent friction, reasonably predicts the wavy flow profile of the undular hydraulic jump. The maximum and minimum depth predictions at the wave crests and troughs compare well with the experiments, as wave amplitude and wave lengths. The computation for $F_1 = 1.31$ are presented in Fig. 2b which highlights however some notable deviations with the physical data. This value of F_1 may be then considered an upper limit for 2D turbulent models in undular jumps, given the possible 3D effects caused by the lateral shockwaves [27,3,13]. Several studies have related the first wave of the undular hydraulic jump to the solitary wave profile [15,2,19,21]. Benjamin and Lighthill [2] obtained a solution for ideal-fluid flows as

$$h'^2 = \frac{6gh^2}{q^2}\left(H_1 - \frac{S_1}{h} - \frac{h}{2} + \frac{q^2}{2gh^2}\right) \tag{17}$$

where $H_1 = h_1 + q^2/(2gh_1^2)$ and $S_1 = (h_1^2/2) + q^2/(gh_1)$. Obviously, only the roots with $h'^2 > 0$ are relevant, corresponding to a solitary wave profile emerging from the upstream uniform supercritical flow [2]. The integral curve of Eq. 17 was considered in Fig. 2 for both $F_1 = 1.08$ and $F_1 = 1.31$. Figure 2 shows that the ideal fluid flow theory can only be used to roughly predict the first wave profile. For $F_1 = 1.31$ the agreement between ideal fluid flow theory and real fluid flow results including wall friction for the first wave crest is reasonable. For the lower value $F_1 = 1.08$, however, the comparison is poor although the ideal fluid flow computations are sometimes considered accurate for F_1 close to unity [15,2,19,21]. The results presented in Fig. 2 suggest that friction should be generally included for a more reasonable prediction of the undular jump profile $h = h(x)$. Note that friction provokes the transition from supercritical to subcritical flow, e.g. the undular hydraulic jump. When there is not friction (potential flow), and in the absence of backwater effects, the flow solution yields the solitary wave profile. Thus, friction results in an undular jump solution, which differ from the potential flow solution.Very few information appears to be available on the free surface characteristics of the undular jump profile. Chanson [9,8] presented a detailed study of the wave amplitude and wavelength based on ideal fluid flow theory. Based on the present results including turbulent friction, a new analysis is developed herein to detail the characteristics of the undular jump profile.

The free surface profile characteristics of the two-dimensional undular jump profile for $F_1 = 1.08$ are considered in Fig. 3. The relation $H/h_c(h/h_c)$ is plotted in Fig. 3a, showing an oscillatory behaviour. For this undular jump $dH/dx > 0$, as deduced from the figure. Further, the parallel flow relation $H/h_c = h/h_c + 0.5(h/h_c)^{-2}$ is included for comparison purposes. A comparison of both curves reveal the limitations of the hydrostatic pressure approach, which does not reproduce the actual flow features of the undular jump profile.

The relation $S/h_c^2(H/h_c)$ is plotted in Fig. 3b where the results are compared with those deduced from the parallel flow relations $H/h_c = h/h_c + 0.5(h/h_c)^{-2}$ and $S/h_c^2 = 0.5(h/h_c)^2 + (h/h_c)^{-1}$. These equations represents in parametric form the boundaries of the Benjamin and Lighthill's diagram [2]. The results for $S/h_c^2(H/h_c)$ including friction are contained inside this diagram, as do are irrotational flows governed by Eq. 17 [15,1]. The justification can be easily extended to real fluid flow in undular jumps by noting in Fig. 3a that at the intersections of the curve $H/h_c(h/h_c)$ from the numerical computation with the hydrostatic curve $H/h_c = h/h_c + 0.5(h/h_c)^{-2}$ results $h'^2 = 2hh''$. Thus, at these points $S/h_c^2 = 0.5(h/h_c)^2 + (h/h_c)^{-1}(1 - h'^2/6)$, always less than the corresponding parallel flow value, thereby resulting in a point $(S/h_c^2, H/h_c)$ inside the cusped part of the Benjamin and Lighthill's diagram.

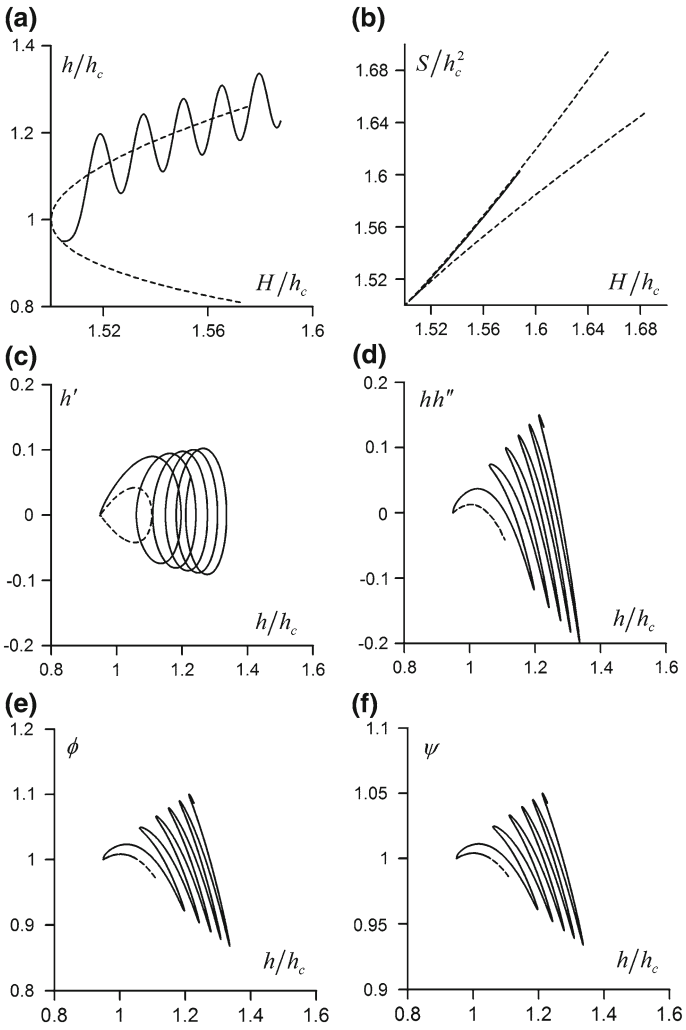

Fig. 3 Undular hydraulic jump profile characteristics for $F_1 = 1.08$ **a** $H/h_c(h/h_c)$ according to (—) Present model, (- - -) Hydrostatic approach, **b** $S/h_c^2(H/h_c)$ from (—) Present model, (- - -) Benjamin and Lighthill's boundaries, **c** $h'(h/h_c)$ from (—) Present model, (- - -) Eq. 17, **d** $hh''(h/h_c)$ (—) Present model, (- - -) ideal fluid flow results, **e** $\phi(h/h_c)$ (—) Present model, (- - -) ideal fluid flow results, **f** $\psi(h/h_c)$ (—) Present model, (- - -) ideal fluid flow results

The relation $h'(h/h_c)$ is plotted in Fig. 3c, where the results are compared with those from Eq. 17 accordingly to ideal fluid flow theory. It can be seen that the magnitude of $h'(h/h_c)$ from real fluid flow computations is generally larger than for ideal fluid flows. Further, the absolute difference between maximum and minimum values of $h'(h/h_c)$ increases with h/h_c. The relation $hh''(h/h_c)$ is plotted in Fig. 3d. As seen therein, the magnitude of $hh''(h/h_c)$ increases considerably with h/h_c. Its value steadily oscillates from positive to negative values accordingly to the pressure field. The results obtained from the solitary wave profile are further included, from which it may be observed that the curvature term is in general lower, in absolute magnitude, than for real fluid flow. Figure 3e contains some numerical data of the

depth-averaged coefficient $\phi(h/h_c)$. It may be observed that this coefficient closely follows the trend observed for $hh''(h/h_c)$. This generally indicates that the contribution of $hh''(h/h_c)$ on $\phi(h/h_c)$ is more relevant than $h'^2(h/h_c)$. When $hh''(h/h_c) < 0$ results $\phi(h/h_c) < 1$, whereas $hh''(h/h_c) > 0$ is associated with $\phi(h/h_c) > 1$. Deviations of $\phi(h/h_c)$ from unity are notable regardless the value of h/h_c. The $\phi(h/h_c)$ values computed from the solitary wave profile are smaller than from real fluid flow results.

Figure 3f includes numerical data of the depth-averaged coefficient $\psi(h/h_c)$. The trend is similar to that reported for $\phi(h/h_c)$, although it may be observed that $|\psi - 1| < |\phi - 1|$.

The free surface profile characteristics of the undular jump profile for $F_1 = 1.31$ are considered in Fig. 4. Figure 4 shows that the trends are essentially as in Fig. 3, yet the order of magnitude of the results is larger. Note also that the terms $hh''(h/h_c)$ and $h'(h/h_c)$ become very large, resulting in extreme values for $\phi(h/h_c)$ and $\psi(h/h_c)$. This excessive drop in both terms $\phi(h/h_c)$ and $\psi(h/h_c)$ roughly indicates a validity limit for the Boussinesq approximation to simulation of undular jump profiles, as previously outlined

So far it was discussed that, for an accurate treatment of undular jumps, the effects of friction are of major relevance. It was shown that, in general, better results may be obtained accounting for friction than when dealing only with ideal fluid flow theory. However, it is still open the question whether the approximation adopted herein for the turbulence friction is reasonable, or not. To further investigate this point, the detailed numerical computations done by Schneider et al. [28] using a k–ε model to integrate the Reynolds equations for undular hydraulic jump flow are considered in Fig. 5, together with experimental results for the same test case.

The corresponding simulation using the present two-dimensional Boussinesq model was included in Fig. 5. It can be seen that the Boussinesq solution allowing for turbulent friction is in excellent agreement with both experimental data and the full integration of the Reynolds equations. Thus, it is confirmed the accuracy of the approximation presented herein, reasonably describing both the relevant effects of friction and streamline curvature in undular hydraulic jumps [13].

4 Undular Weir Flow

The undular weir flow is a transitional free surface flow from subcritical $F < 1$ to supercritical $F > 1$ flow in the form of an undulating flow profile. The undular flow over a rough broad-crested weir is considered in Fig. 6 [25,29]. Equations 11 and 12 were integrated numerically using a 4th-order Runge-Kutta method with $H_o/h_c = 1.626$, where H_o = approach flow energy head. The boundary conditions used were the test data at the first wave trough: i.e., $h/h_c = 1.196$ and $h' = 0$. The friction slope dH/dx was determined using a Bazin roughness coefficient of 0.41 [29]. The results for $h = h(x)$ are compared with test data in Fig. 6, resulting in excellent agreement both for the wave crests and troughs. Equation 12 for $dH/dx = 0$, e.g. ideal fluid-flow, was similarly considered using the same boundary conditions. The result is also plotted in Fig. 6, showing a cnoidal wave train. These results indicate that, from the ideal-fluid flow solution of Eq. 12, there is not any possible transition from subcritical $F < 1$ to supercritical $F > 1$, whereas the inclusion of the friction term allows for the establishment of transitional flow in the vicinity of the overfall brink. Further, the theoretical result predicts correctly the downstream boundary condition, corresponding to a free overfall.

The free surface profile characteristics of the undular weir profile are considered in Fig. 7. The relation $H/h_c(h/h_c)$ is plotted in Fig. 7a, showing an oscillatory behaviour. It is seen that both the initial and downstream sections of the flow profile have non-hydrostatic flow

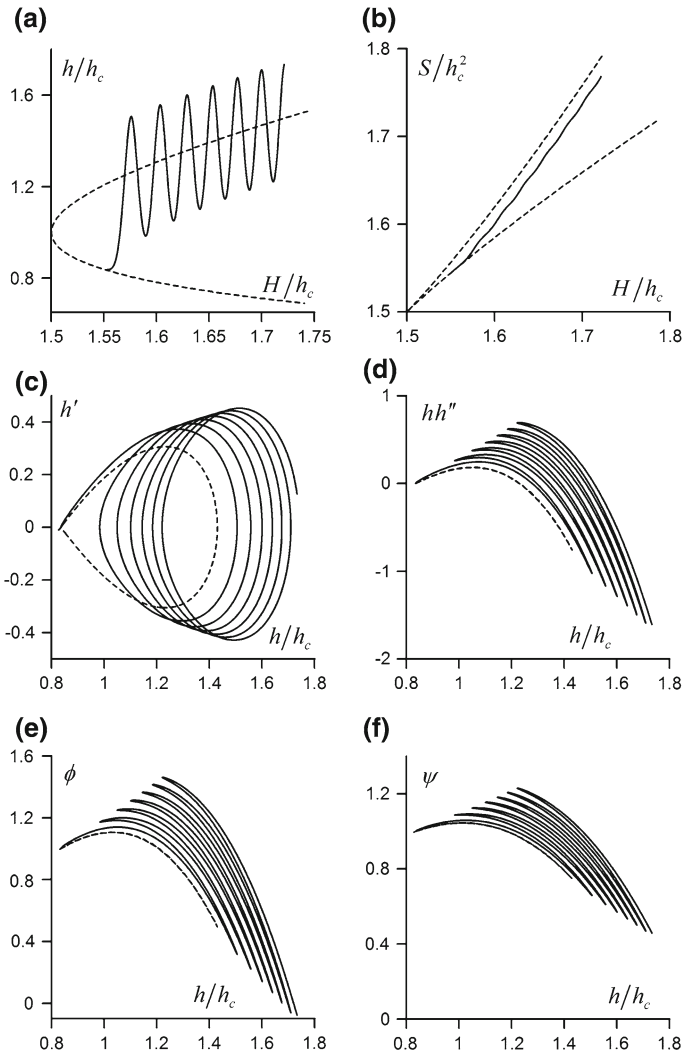

Fig. 4 Undular hydraulic jump profile characteristics for $F_1 = 1.31$ **a** $H/h_c(h/h_c)$ according to (—) Present model, (- - -) Hydrostatic approach, **b** $S/h_c^2(H/h_c)$ from (—) Present model, (- - -) Benjamin and Lighthill's boundaries, **c** $h'(h/h_c)$ from (—) Present model, (- - -) Eq. 17, **d** $hh''(h/h_c)$ (—) Present model, (- - -) ideal fluid flow results, **e** $\phi(h/h_c)$ (—) Present model, (- - -) ideal fluid flow results, **f** $\psi(h/h_c)$ (—) Present model, (- - -) ideal fluid flow results

conditions, departing from the parallel flow relation $H/h_c = h/h_c + 0.5(h/h_c)^{-2}$. Note also that the flow conditions at the free overfall results in $H/h_c < 1.5$ and $h/h_c < 1$. The relation $S/h_c^2(H/h_c)$ obtained from the numerical results is plotted in Fig. 7b along with the Benjamin and Lighthill's (1954) boundaries. Note that the undular weir flow profile is not fully contained inside the cusped part of the diagram. Benjamin and Lighthill [2] and Benjamin [1] stated that all irrotational wave motions should lie inside this cusped part. The present results indicate that, when friction is included in the analysis, this is not generally valid. Noteworthy the undular jumps studied in the previous section did lie inside, despite

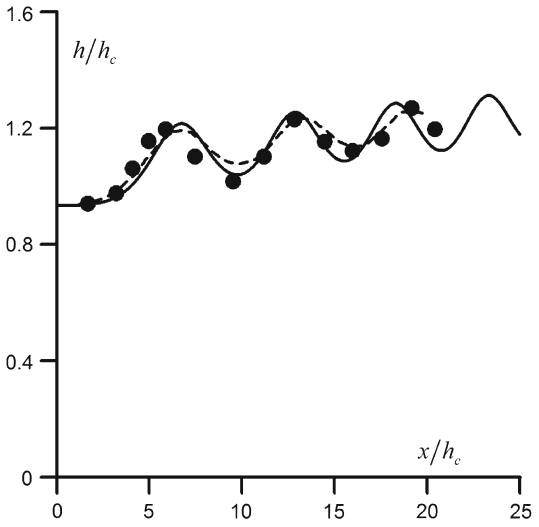

Fig. 5 Undular hydraulic jump profile $h/h_c(x/h_c)$ for $F_1 = 1.11$, $R_1 = 93000$, $S_o = 1/282$ from (—) Present model, (- - -) Integration of Reynolds equations with k–ε model [28] and (•) Experimental data [28]

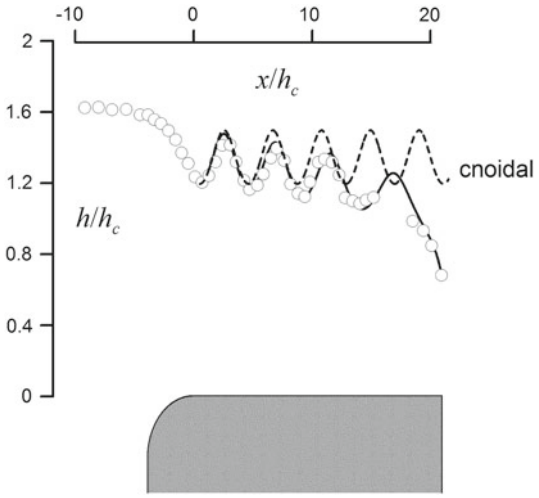

Fig. 6 Transition from $F < 1$ to $F > 1$: undular weir flow profile $h/h_c(x/h_c)$ for $H_o/L = 0.078$ from (—) Real fluid flow theory, (- - -) Ideal fluid flow, (○) experimental data [29]

the inclusion of friction. The relation $h'(h/h_c)$ is plotted in Fig. 7c where the results are compared with those from the cnoidal wave solution. It is seen that the results are not in agreement, especially for $h/h_c < 1$, when the flow approaches the free overfall. The relation $hh''(h/h_c)$ is plotted in Fig. 7d, again with evident deviations from the cnoidal wave train for $h/h_c < 1$. Figure 7e and f contain the numerical data in terms depth-averaged coefficients $\phi(h/h_c)$ and $\psi(h/h_c)$, showing some notable deviations from unity. These results confirm the strong deviation of pressure conditions from the hydrostatic law at the free overfall.

Flow over a broad-crested weir implies a developing boundary layer over the weir crest [17,18]. When the surface profile is free from undulations the boundary layer displacement thickness $\delta^* = \delta^*(x)$ may be simply approximated by power-type functions resulting from zero-pressure gradient models [17,31,18]). The boundary layer frictional effects for a

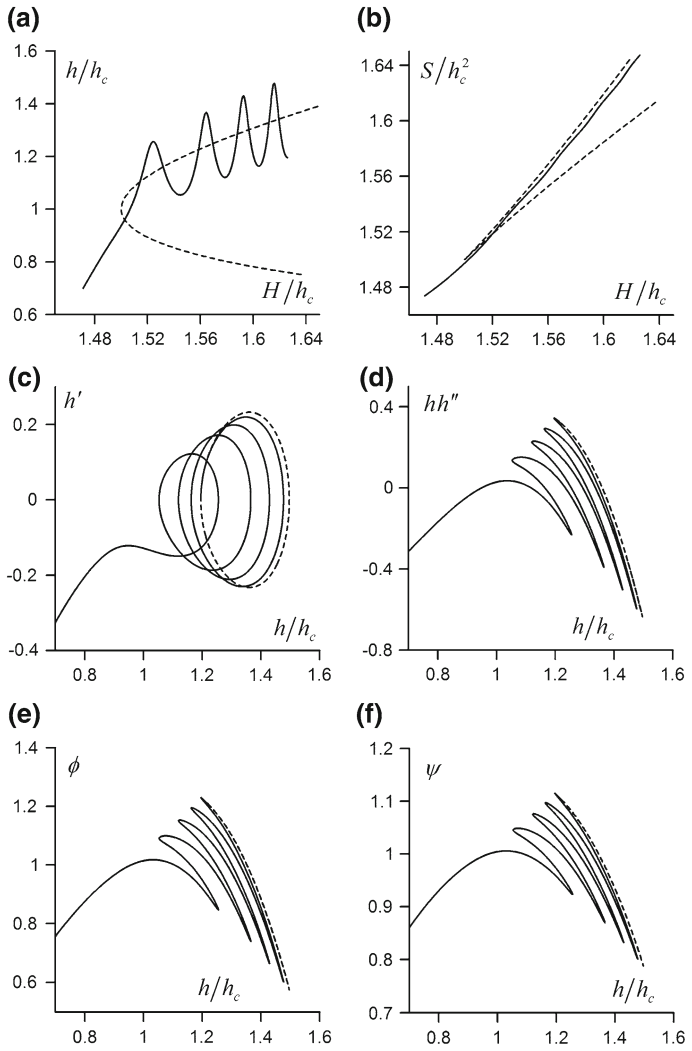

Fig. 7 Undular weir flow profile characteristics for $H_o/L = 0.078$ **a** $H/h_c(h/h_c)$ according to (—) Present model, (- - -) Hydrostatic approach, **b** $S/h_c^2(H/h_c)$ from (—) Present model, (- - -) Benjamin and Lighthill's boundaries, **c** $h'(h/h_c)$ from (—) Present model, (- - -) Eq. 17, **d** $hh''(h/h_c)$ (—) Present model, (- - -) ideal fluid flow results, **e** $\phi(h/h_c)$ (—) Present model, (- - -) ideal fluid flow results, **f** $\psi(h/h_c)$ (—) Present model, (- - -) ideal fluid flow results

zero-pressure gradient boundary layer flow are accounted for by introducing the von-Kármán integral equation as [31]

$$\frac{\mathrm{d}\theta}{\mathrm{d}x} = \frac{C_f}{2} \tag{18}$$

where θ = boundary layer momentum thickness, $C_f = \tau_o/(\rho U_M^2/2) = f/4$ = skin-friction coefficient, U_M = maximum (subscript M) velocity at boundary layer edge and τ_o = boundary shear stress. Harrison [18] developed an approach based on Granville's C_f chart,

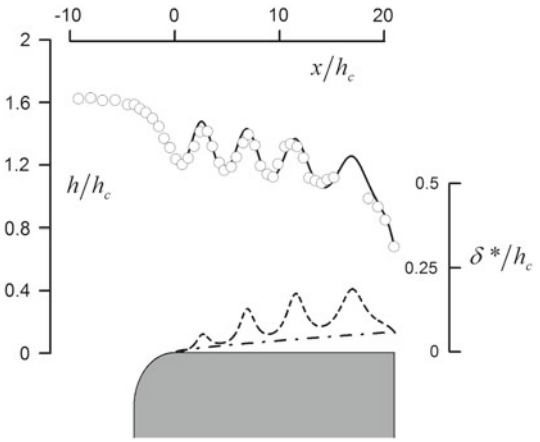

Fig. 8 Transition from F < 1 to F > 1: undular weir flow for $H_o/L = 0.078$: $h/h_c(x/h_c)$ from (—) Theory, (∘) experimental data [29], $\delta^*/h_c(x/h_c)$ from (- - -) undular free surface flow approach, (— - —) zero-pressure gradient model

from which θ and δ^* may be deduced. However, for undular weir flow the pressure gradient steadily changes accordingly to Eq. 6 form favourable to adverse, and vice-versa, thereby affecting the growth conditions of the boundary layer. In these conditions Eq. 18 does not reproduce the actual flow features, as discussed below. There are few attempts in the literature with considerations about the boundary layer in weir flow, where the potential flow results in appreciable streamline curvature. In these conditions the potential flow above the boundary layer implies high flow curvature, and the velocity distribution may be approximated by [27]

$$V = V_s \exp\left(-hh''\frac{1-\eta^2}{2}\right) \tag{19}$$

where V_s = free surface velocity. The definition of the boundary layer thickness δ^* in flows with curvature may be formulated based on the integral of the potential velocity distribution as

$$q = \int_{\delta^*}^{h} \frac{V}{\cos i} d\eta \tag{20}$$

where i = streamline inclination. Inserting Eq. 19 into Eq. 20, and assuming a linear variation for $i = i(\eta)$, results after an approximate integration similar to Montes and Chanson [27]

$$H_o = h + \frac{q^2}{2g\,(h-\delta^*)^2}\left(1 + \frac{2hh'' - h'^2}{3}\right) \tag{21}$$

Using the results for the flow profile $h = h(x)$ obtained from the approximate Reynolds-averaged model Eqs. 11 and 12, the energy equation for the potential flow above the boundary layer Eq. 21 may be used to estimate the profile $\delta^* = \delta^*(x)$.

The results obtained for the boundary layer thickness development in undular weir flow are plotted in Fig. 8. They show that the profile $\delta^* = \delta^*(x)$ is undular in response to the oscillatory pressure gradient resulting from the Boussinesq terms h'^2 and hh''. Thus, the effects of the pressure gradient on the boundary layer development for undular weir flow are important. This may be further highlighted by comparing the present the results with those obtained using a zero-pressure gradient boundary layer model. The method proposed by Harrison [18] was applied to the present test case and the result of the numerical simulation

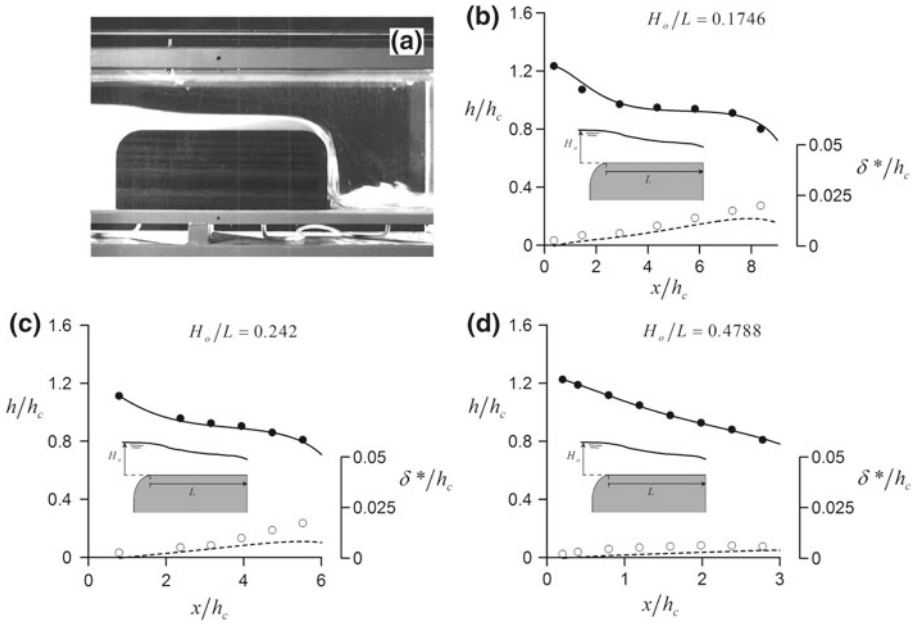

Fig. 9 Transition from F < 1 to F > 1: **a** Round-nosed broad-crested weir, **b–d** $h/h_c(x/h_c)$ from (—) Present theory, (•) experimental data [30],$\delta^*/h_c(x/h_c)$ from (- - -) undular free surface flow approach, (○) zero pressure gradient estimation [30]

for $\delta^* = \delta^*(x)$ is included in Fig. 8. It is of interest to remark that the value of $\delta^* = \delta^*(x = L)$ is of similar magnitude from both methods. However, the boundary layer profile for undular flow generally deviates from the standard equations used in broad-crested weir flow assuming parallel streamlines. This indicates the complex real fluid flow features of undular flow over broad-crested weirs, given by its undulating boundary layer development.

Model test data in a horizontal broad crested weir with a rounded upstream nose (see Fig. 9a) of 10 cm [30] are plotted in Fig. 9 for three different dimensionless upstream heads H_o/L. The comparison between the present theory and model data was conducted by solving the system of differential Eqs. 11 and 12 for the unknowns $h(x)$ and $H(x)$ with a 4th-order Runge-Kutta method. The boundary conditions are taken at the first experimental point of the free surface profile. The computational results are also included in Fig. 9, showing an excellent agreement with observations. The first point that deserves consideration is that the flow surface $h = h(x)$ of the broad-crested weir shows a considerable slope h' and curvature h'' in a great extension of the crest length, for a wide range of operational heads. The flow profile of broad-crested weir flow results in a cnoidal wave type profile for $H_o/L < 0.15$ [26], see Fig. 8. For $0.15 < H_o/L < 0.33$ the flow is an incomplete cnoidal wave profile, as shown herein in Fig. 9. In these cases, only one inflexion point in the flow profile is seen and no full waves are present. When $H_o/L \approx 0.5$ the flow profile is almost a straight and sloped drawdown curve from the inlet flow depth up to the free overfall brink depth (Fig. 9d). Thus, broad-crested weir flow for $H_o/L < 0.15$ is governed by cnoidal wave theory, associated with non-hydrostatic conditions and a marked wave type free surface. For $H_o/L > 0.5$ the flow surface is almost a straight drawdown curve, associated also with non-hydrostatic conditions. In the interval of operation heads $0.15 < H_o/L < 0.33$, however, it is possible

to find a small region of the crest length L where quasi-parallel streamline flow prevails, as observed in both Fig. 9b and c.

The results for $\delta^* = \delta^*(x)$ using Eq. 21 are included in Fig. 9. These results are compared with the values deduced by Vierhout [30] from his test data using a zero-pressure gradient approach. As shown in Fig. 9b and c, the zero-pressure gradient approach is reasonable for a major part of the weir crest given its agreement with the more general relationship Eq. 21 accounting for the pressure gradient effects. There is however a lack of agreement in the flow domain near the overfall brink where the pressure gradient is significant and the zero-pressure gradient boundary layer methods are unreliable. For the test case of Fig. 9d, the relation H_o/L is high, and boundary layer effects are of minor relevance as observed from the thin displacement thickness obtained in this case. This confirms that $H_o/L \approx 0.5$ may be considered as a limit above which the discharge characteristics are mainly dominated by the streamline curvature. The round-nosed broad crested weir is a water discharge measurement structure. The new method for the boundary layer computation supports, then, the use of zero-pressure gradient computation under conditions of parallel-streamline flow at the crest. However, it further reveals that the discharge estimation may not be accurate if the zero-pressure gradient method is applied beyond the limits indicated in the present results.

Further, it appears necessary to investigate additional flow types in the Benjamin and Lighthill's diagram $S/h_c^2(H/h_c)$. The undular weir flow was shown herein to result in points outside the diagram, thereby indicating that real fluid flows may not lie necessarily inside. However, still remains the question whether all irrotational motions will lie inside, or not, as proposed by Benjamin [1]. The critical flow over a round-crested weir is considered herein as an additional test case. At the weir crest, critical flow conditions prevail, and H and S are given respectively by

$$H = h + \frac{q^2}{2gh^2}\left(1 + \frac{2hh'' - h'^2}{3} + hz''\right) \tag{22}$$

and

$$S = \frac{h^2}{2} + \frac{q^2}{gh}\left(1 + \frac{hh'' - h'^2}{3} + \frac{hz''}{2}\right) \tag{23}$$

with $z'' =$ crest curvature. The analysis of the experimental data of Blau by Montes [26] was used to evaluate H and S at the crest of parabolic weirs, and the results are plotted in Fig. 10, with the numerical results for the undular weir flow test case. Interestingly, the data pairs $(S/h_c^2, H/h_c)$ computed for critical flow over round-crested weirs lie outside the Benjamin and Lighthill's diagram, with values significantly less than 1.5. The flow over a round-crested weir is irrotational, and, thus, present results indicate that all irrotational motions do not lie inside the Benjamin and Lighthill's diagram. Further, when data for critical flow over round-crested weirs is considered simultaneously with undular weir flow data, they appear to be highly correlated in the $S/h_c^2(H/h_c)$ plane (Fig. 10). Both types of flows are transitions from $F < 1$ to $F > 1$, possibly indicating a unique feature of these flow types. By contrast, transitions from $F > 1$ to $F < 1$, as in the undular jump, appear to lies always inside the cusped part of Benjamin and Lighthill's diagram, despite friction effects. Note that the points in Fig. 10 for undular weir flow refer to the computed free surface $h = h(x)$ for a given discharge, whereas for the round-crested weir flow the points refer to the discharge curve obtained at the weir crest section ($z' = 0$) under different discharges.

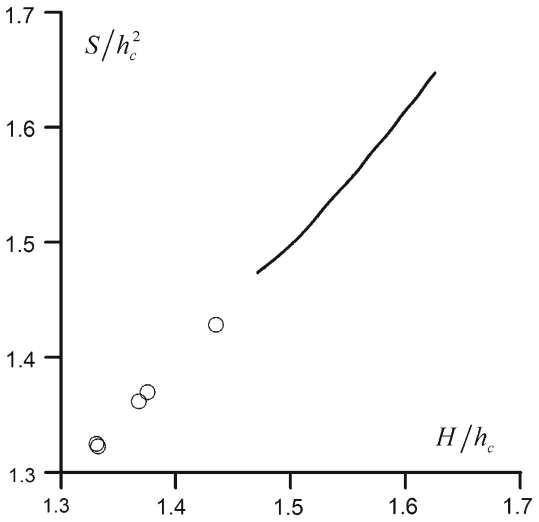

Fig. 10 Transition from F < 1 to F > 1 in the $S/h_c^2(H/h_c)$ plane: (—) Undular weir flow, (○) Round-crested weir flow

5 Conclusion

In the present research two open channel flows types with near-critical flow conditions were studied based on a Boussinesq-type energy equation allowing for friction effects: i.e., the undular hydraulic jump and the undular weir flow.

The results of the present approach for the undular hydraulic jump were compared with experimental data, and showed some good agreement. Further, the results were compared with irrotational flow solutions, resulting in systematic deviations, thereby indicating that the ideal fluid flow computations should be used with caution for undular jumps. Some flow features of the undular jump profile such as free surface slope, curvature, specific energy diagram, Benjamin and Lighthill's diagram and depth-averaged energy and momentum coefficient were detailed based on the new results presented herein. The present model results were also compared with the full integration of the Reynolds equations for turbulent flow in an undular hydraulic jump, resulting in an excellent agreement.

The present model was further applied to the undular weir flow over broad-crested weirs. The results compared favourably to physical observations. The flow features of the boundary layer development on the broad-crested weir were shown to be oscillating, in response to the steady changing pressure gradient from favourable to adverse, and viceversa. The results for the undular boundary layer flow were compared with a numerical approach for the boundary layer development for a zero pressure gradient flow. The comparative analysis showed some large deviations, indicating the unique features of the shear flow development under an undular free surface. Thus, existing models for boundary layer development on broad-crested weirs are limited, and may not be used when the pressure gradient results in an undular free surface.

The flow results for both undular hydraulic jump and undular weir flow were plotted in the so-called Benjamin and Lighthill's plane $S/h_c^2(H/h_c)$. All irrotational wavy flows were assumed previously to lie inside the cusped part of this plane bounded by the loci of parallel-streamline flows. However, the present results for the undular weir flow showed that this feature is not general when a friction term is included in the analysis, although the results for undular hydraulic jumps were opposite. The data for irrotational critical flow over

round-crested weirs were further considered as a flow type near the critical depth, resulting in points largely outside the cusped part. Thus, it is believed that neither near-critical undular flows allowing for friction, nor irrotational flow over weirs near the critical depth, lie necessarily inside the cusped part of the $S/h_c^2(H/h_c)$ plane. However, it was found that the undular hydraulic jump, a transition from $F > 1$ to $F < 1$, lies inside, while both the undular weir flow and the round-crested weir flow, transitions from $F < 1$ to $F > 1$, lie outside. This appears to indicate that the type of flow transition is relevant relative to the $S/h_c^2(H/h_c)$ relation, while the physical explanation needs further research.

Acknowledgments The first Author was supported by a contract of modality JAE-DOC of the program "Junta para la Ampliación de Estudios", CSIC, National Research Council of Spain, co-financed by the FSE.

References

1. Benjamin TB (1995) Verification of the Benjamin-Lighthill conjeture about steady water waves. J Fluid Mech 295:337–356
2. Benjamin TB, Lighthill MJ (1954) On cnoidal waves and bores. Proc Roy Soc London A 224:448–460
3. Ben meftah M, De Serio F, Mossa M, Pollio A (2007) Analysis of the velocity field in a large rectangular channel with lateral shockwave. Environ Fluid Mech 7(6):519–536
4. Boussinesq J (1877) Essai sur la théorie des eaux courantes. Mémoires présentés par divers savants à l'Académie des Sciences, Paris 23, 1–680 (in French)
5. Bose SK, Dey S (2007) Curvilinear flow profiles based on Reynolds averaging. J Hydraul Eng 133(9):1074–1079
6. Castro-Orgaz O (2010) Steady open channel flows with curved streamlines: the Fawer approach revised. Environ Fluid Mech 10(3):297–310
7. Chanson H (1995) Flow characteristics of undular hydraulic jumps: comparison with near-critical flows. Res Rep CH 45/95. Dept Civ Eng, University of Queensland, Brisbane Australia
8. Chanson H (1995) Broad-Crested Weir—discussion. J Irrig Drain Eng ASCE 121(2):222–224
9. Chanson H (1996) Free surface flows with near critical flow conditions. Can J Civ Eng 23(6):1272–1284
10. Chanson H (2004) The hydraulics of open channel flows: an introduction. Butterworth-Heinemann, Oxford, UK
11. Chanson H (2009) Current knowledge in hydraulic jumps and related phenomena. A survey of experimental results. Eur J Mech B/Fluids 28(2), 191–210. (doi:10.1016/j.euromechflu.2008.06.004)
12. Chanson H (2009) Applied hydrodynamics: an introduction to ideal and real fluid flows. CRC Press, Taylor & Francis Group, Leiden, The Netherlands, 478 pp
13. Chanson H, Montes JS (1995) Characteristics of undular hydraulic jumps: experimental apparatus and flow patterns. J Hydraul Eng 121(2):129–144; Discussion: 1997, 123(2): 161–164
14. Darcy HPG, Bazin H (1865) Recherches Hydrauliques. (Hydraulic Research.) Imprimerie Impériales, Paris, France, Parties 1ère et 2ème (in French)
15. Fawer C (1937) Etude de quelques écoulements permanents à filets courbes. Thesis. Université de Lausanne. La Concorde, Lausanne, Switzerland (in French)
16. George WK (2006) Recent advancements towards the understanding of turbulent boundary layers. AIAA J 44(11):2435–2449
17. Harrison AJM (1967) The streamlined broad crested weir. In: Proceedings of the institution of civil engineers, London, England, 38: 657–678
18. Harrison AJM (1967) Boundary layer displacement thickness on flat plates. J Hydraul Div 93(4):79–91
19. Iwasa Y (1955) Undular jump and its limiting conditions for existence. In: Proceedings of the 5th Japan National Congress Applied Mech II-14:315–319
20. Koch C, Chanson H (2008) Turbulent mixing beneath an undular bore front. J Coast Res 24(4):999–1007
21. Mandrup-Andersen V (1978) Undular hydraulic jump. J Hydraul Div ASCE 104(HY8):1185–1188; Discussion: 105(HY9): 1208–1211
22. Marchi E (1963) Contributo allo studio del risalto ondulato. Giornale del Genio Civile 101(9):466–476
23. Matthew GD (1963) On the influence of curvature, surface tension and viscosity on flow over round-crested weirs. In: Proceedings of the institution of civil engineers, London, England, 25: 511–524. Discussion: 1964, 28:557–569

24. Matthew GD (1991) Higher order, one-dimensional equations of potential flow in open channels. In: Proceedings of the institution of civil engineers, London, England, 91:187–201
25. Montes JS (1986) A study of the undular jump profile. 9th Australasian Fluid Mech Conf, Auckland, 148–151
26. Montes JS (1998) Hydraulics of open channel flow. ASCE Press, Reston, VA
27. Montes JS, Chanson H (1998) Characteristics of undular hydraulic jumps: experiments and analysis. J Hydraul Eng 124(2):192–205
28. Schneider W, Jurisits R, Bae YS (2009) An asymptotic iteration method for the numerical analysis of near-critical free-surface flows. In: 14th International conference on fluid flow technologies: conference on modelling fluid flow, Budapest, 8 pp
29. Serre F (1953) Contribution à l'étude des écoulements permanents et variables dans les canaux. La Houille Blanche 8(6–7):374–388; 8(12):830–887 (in French)
30. Vierhout MM (1973) On the boundary layer development in rounded broad-crested weirs with a rectangular control section. Res Rep no 3. Laboratory of Hydraulics and Catchment Hydrology, Agricultural University of Wageningen, The Netherlands
31. White FM (1991) Viscous fluid flow. McGraw-Hill, New York